PALAIOS
Emphasizing the impact of life on Earth's history

PALAIOS, 2012, v. 27, p. 317–325
Research Article
DOI: 10.2110/palo.2011.p11-093r

PRESERVATION OF GIANT ANOMALOCARIDIDS IN SILICA-CHLORITE CONCRETIONS FROM THE EARLY ORDOVICIAN OF MOROCCO

ROBERT R. GAINES,[1]* DEREK E.G. BRIGGS,[2,3] PATRICK J. ORR,[4] and PETER VAN ROY[2,5]

[1]*Geology Department, Pomona College, 185 East Sixth Street, Claremont, California 91711, USA, robert.gaines@pomona.edu;* [2]*Department of Geology and Geophysics, Yale University, New Haven, Connecticut 06520, USA, derek.briggs@yale.edu, peter.vanroy@yale.edu;* [3]*Yale Peabody Museum of Natural History, Yale University, New Haven, Connecticut 06520, USA;* [4]*University College Dublin School of Geological Sciences, University College Dublin, Dublin 4, Ireland, Patrick.Orr@ucd.ie;* [5]*Research Unit Palaeontology, Department of Geology and Soil Science, Ghent University, Krijslaan 281/S8, B-9000, Ghent, Belgium*

ABSTRACT

The recently discovered Fezouata Biota, from the Early Ordovician (late Tremadocian to late Floian) of Morocco, preserves a diverse soft-bodied fauna. While preservation is mostly of Burgess Shale-type, giant anomalocaridids also occur in siliceous concretions. Petrographic and geochemical analyses of these concretions reveal their growth history and the circumstances that led to the fossilization of nonbiomineralized anatomy within them. The large (>1 m) concretions are homogeneous in composition and geochemical characteristics, suggesting rapid, pervasive growth of mineral frameworks during decay of the large animals at, or near, the sediment-water interface. Concretions are comprised of ultrafine-grained (2–20 μm) authigenic quartz, Fe chlorite, and calcite, a composition unlike other described marine concretions. Abundant pyrite, now represented by oxide pseudomorphs, grew adjacent to the anomalocaridid carcasses, but rarely within the matrix of the concretions. This distribution indicates that sulfate reduction around the carcasses was vigorous within otherwise organic-poor sediments resulting in the establishment of prominent chemical gradients around the giant anomalocaridids that led to early precipitation of mineral overgrowth around nonbiomineralized tissues. Rapid precipitation of intergrown silica and Fe chlorite required an abundant source of silica, iron, and aluminum. These ions were likely derived from dissolution of volcanic ash in the sediments. Limited intergrown calcite ($\delta^{13}C$ avg. −12.2‰, n = 23) precipitated from bicarbonate that was generated largely by sulfate reduction of organic tissues of the carcasses. Whereas Burgess Shale-type preservation of fossils in the Fezouata biota required suppression of degradation, exceptional preservation of anomalocaridids within the siliceous concretions resulted from extensive microbial decomposition of a large volume of organic tissues. Rapid mineralization was facilitated by localization of microbial activity around the large carcasses and must have required an unusually reactive sediment composition.

INTRODUCTION

The lower and upper Fezouata Formations of Morocco preserve a remarkable record of Early Ordovician diversity during a critical interval in the history of life when soft-bodied preservation is very rare (Van Roy et al., 2010). The great majority of soft-bodied fossils within these formations are preserved in mudstone as two-dimensional compressions. Preservation of these fossils (Van Roy et al., 2010) appears to be of Burgess Shale type (see Butterfield, 2003). Giant anomalocaridids, however, occur within large siliceous concretions at a single horizon in the uppermost part of the lower Fezouata Formation (Figs. 1, 2A–C; Van Roy and Briggs, 2011). These giant specimens are particularly important not only because of their age, but also because they retain three-dimensional detail of some aspects of fossil anatomy that were lost during fossilization of anomalocaridids preserved as compressions in Fezouata mudstones and in older (Cambrian) Burgess Shale-type deposits. Dorsal arrays of flexible blades, interpreted as gills, are preserved in three-dimensional relief within the concretions, offering new insights into the paleoecology and functional morphology of anomalocaridids (Van Roy and Briggs, 2011, figures therein). The presence of large concretions within a mudstone succession that yields soft-bodied compression fossils presents a paradox: whereas abundant soft-bodied preservation in mudstone above and below the concretion-bearing interval required the suppression of normal decay (Butterfield, 1995; Petrovich, 2001; Gaines et al., 2005, 2008), the growth of concretions typically involves extensive microbial decomposition of organic matter (e.g., Berner, 1968; Raiswell, 1987).

Many concretions are thought to grow slowly over timescales of millennia (e.g., Sellés-Martínez, 1996; Raiswell and Fisher, 2000). Concretions bearing soft-bodied fossils, in contrast, which are known from numerous localities of different geologic ages (Mapes, 1987; Martill, 1988; Wilby and Martill, 1992; Park, 1995; Huggett et al., 2000; Orr et al., 2000; Raiswell and Fisher, 2000; Briggs, 2003; Maas et al., 2006; Zhang et al., 2007; Maeda et al., 2011), must have involved rapid mineralization prior to the degradation of soft tissues (Briggs and Kear, 1994; Sagemann et al., 1999). This interpretation is supported by the study of concretions forming in modern marginal-marine environments (Allison and Pye, 1994; Pye et al., 1990). Exceptional preservation via molds or replacement commonly occurs within carbonate concretions composed of either calcite or siderite (Orr et al., 2000), but is rarer in siliceous concretions. An important early terrestrial fauna is preserved in hot spring silica sinter deposits of the Lower Devonian Rhynie Chert (Rice et al., 2002). Entombment in silica in marine settings is largely a Proterozoic phenomenon and typically preserves only microbial fossils (Schopf, 1993) or acritarchs (Xiao et al., 2010). The Middle Cambrian Conasauga Formation yields algae, sponges, and the problematic pseudofossil(?) *Brooksella* preserved in three-dimensions in concretions, but the Conasauga fossils are preserved by silica infilling and replacement rather than by mineral overgrowth around soft tissues (Ciampaglio et al., 2006; Schwimmer and Montante, 2007). The preservation of soft-bodied macrofossils within siliceous concretions in marine environments is exceptionally rare.

Herein, we report the results of mineralogic, textural, and geochemical analyses of the Fezouata concretions. We describe the paragenesis of the concretions and the pathway for the preservation of anomalocaridids within them.

GEOLOGIC SETTING

In the area to the north of Zagora, the lower and upper Fezouata Formations of the eastern Anti-Atlas of Morocco comprise a thick (>1000 m) succession of mudstone deposited in a deep-water setting (Fig. 1; Van Roy et al., 2010). The formations were deposited during the Early Ordovician (late Tremadocian–late Floian) on a rifted margin of present-day northwestern Africa that formed after the separation of

* Corresponding author.
Published Online: May 2012

 0883-1351/12/0027-317$3.00

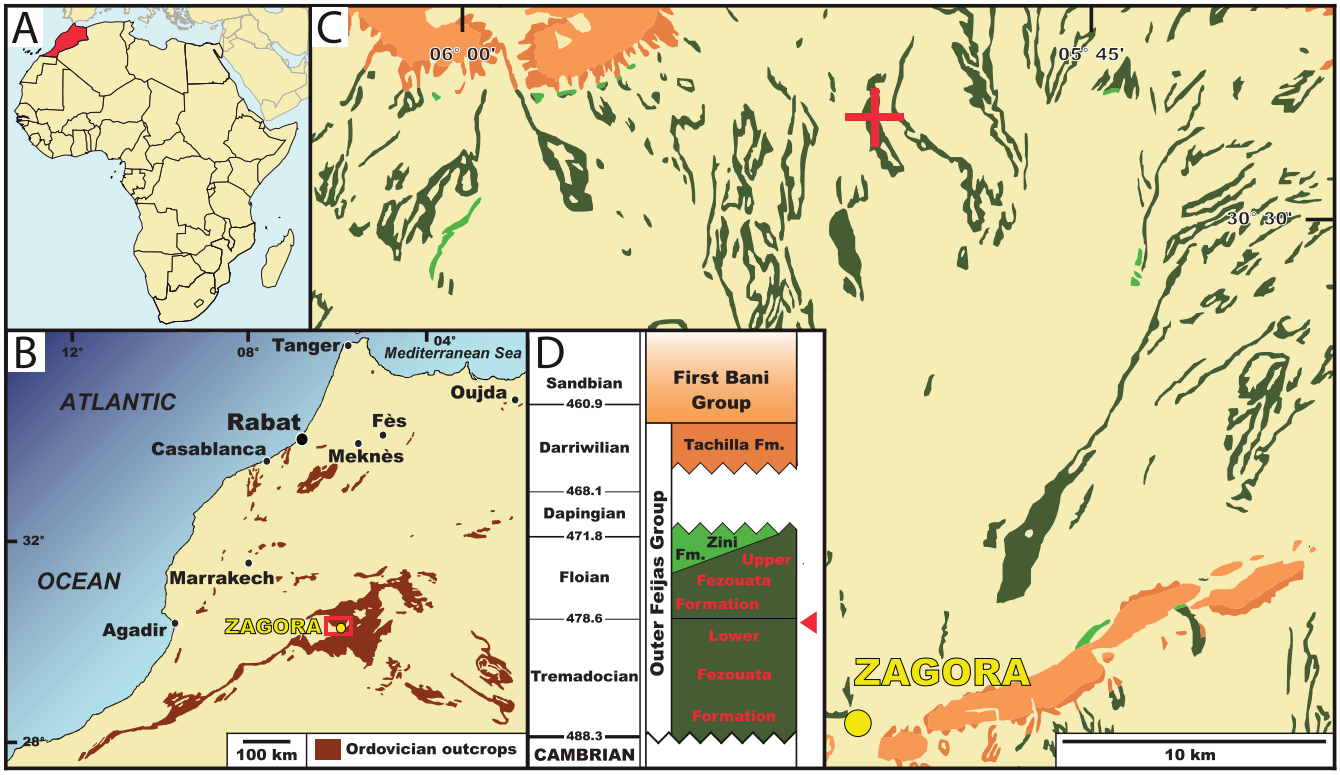

FIGURE 1—Location map and stratigraphic column. A) Map of Africa with the location of Morocco highlighted in red. B) Context map showing the location of the study area within northwestern Africa. C) Location map of the study area, concretion locality is marked with a red +. The distribution of geologic units is shown, colors indicated on the stratigraphic column in D. D) Schematic stratigraphic column of the Ordovician strata in the study area. Concretion-bearing horizon is indicated by a red triangle.

Avalonia from West Gondwana in the earliest Ordovician (Cocks and Torsvik, 2006). The region was situated at high latitude near the South Pole, although a global greenhouse climate prevailed and continental glaciers were not present (Cocks and Torsvik, 2006; Finnegan et al., 2011). The sedimentology and depositional context of the succession awaits detailed investigation.

Siliceous concretions that preserve specimens of giant anomalocaridids were discovered within mudrock in a single horizon of the uppermost part of the lower Fezouata Formation (Van Roy and Briggs, 2011). This part of the section is interpreted to have accumulated below storm wave base (Van Roy et al., 2010).

MATERIAL AND METHODS

Samples were obtained from two large concretions (Figs. 2A–C) that preserve giant, articulated anomalocaridids (Van Roy and Briggs, 2011). The concretions were collected at a locality approximately 20 km north of Zagora, Morocco (Fig. 1), and are held by the Peabody Museum at Yale University. They split along the fossils, which are aligned with the long axes of the concretions (the plane of the fossil lies closer to one surface of the concretion than the other). Only the part (convex upward) of the larger example (YPM 226437 part), referred to here as concretion 1 (Fig. 2A; Van Roy and Briggs, 2011, fig. 1a), was analyzed. This concretion is 98 cm long. The anomalocarid, preserved only partially, occurs across its entire length. The maximum thickness, measured normal to the plane of the fossil, is ~17.5 cm in the part and ~7 cm in the counterpart. Both part and counterpart of a second, incomplete concretion specimen (YPM 226438), referred to here as concretion 2 (Figs. 2B–C), were analyzed. The maximum length of this concretion, which preserves only a portion of the trunk, is 43 cm: the size of the preserved segments indicates that this animal was similar in size to the first specimen. The maximum thickness, measured normal to the plane of the fossil, is ~15 cm on the part and ~10.5 cm on the counterpart. The three pieces analyzed from the two concretions were cut approximately perpendicular to the fossil providing a radial (center-to-edge) transect. A fourth fragment was also obtained from broken material from an unknown position within concretion 1. A third incomplete concretion (YPM 226639: Van Roy and Briggs, 2011, fig. S3a) was not analyzed. It is 56 cm long: the maximum thickness, measured normal to the plane of the fossil, from the edge to the fossil is ~8.5 cm on the part and ~9.5 cm on the counterpart.

Each of the three large pieces, designated A (concretion 1, part), B (concretion 2, part) and C (concretion 2, counterpart), was slabbed parallel to the transect, polished, and prepared for X-radiography, acetate peeling, and thin sectioning. Portions of the three pieces were divided at ~1 cm intervals along the center-to-edge transects, yielding a total of 22 samples. Samples were numbered sequentially from center (A1, B1, C1) to the edge (A12, B5, C5). Whole-rock powders (n = 23) were prepared from each of these samples and from the isolated fragment of concretion 1 (YPM 226437) and subjected to X-ray diffraction (XRD), X-ray fluorescence (XRF) and carbon and oxygen isotope analysis. Approximately 2 cm^3 of each sample was ground by hand in a mortar and pestle and digested in 37% HCl for 48 hours at room temperature. The insoluble residues were examined using a binocular microscope and a scanning electron microscope (SEM). The remaining parts of each sample were prepared for SEM textural analysis by polishing or by breaking to expose fresh surfaces.

Powders of each sample (n = 23) were analyzed for mineralogy using a Rigaku Ultima IV X-Ray Diffractometer at Pomona College. Samples were scanned over a range of 10° to 65° 2θ, with a scanning speed of 5° per minute and a sampling interval of 0.02°. Diffraction patterns were analyzed with the aid of the JADE 8.0 software package.

Whole-rock powders from each sample were dissolved in phosphoric acid and analyzed online for $\delta^{13}C$ and $\delta^{18}O$ using a Thermo Finnigan

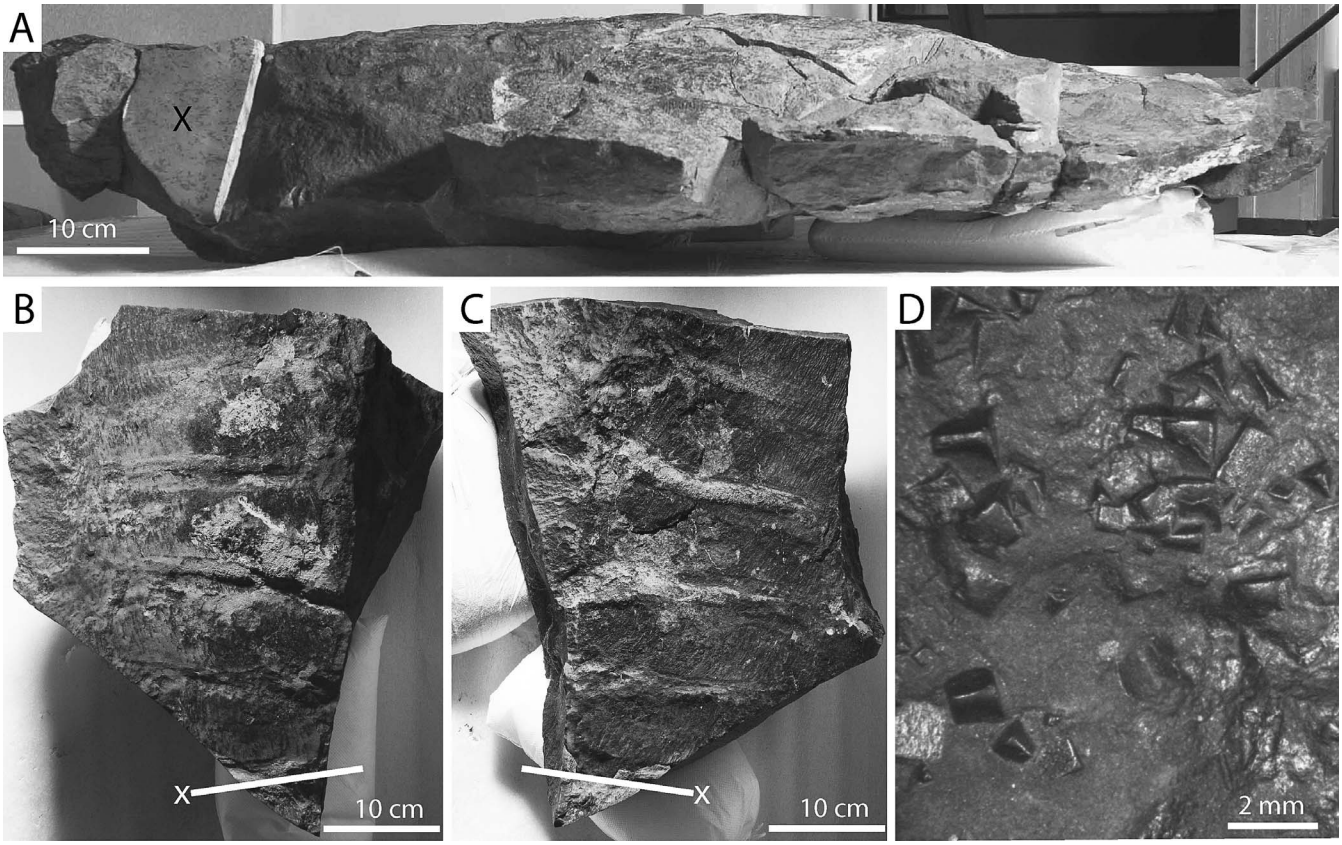

FIGURE 2—A) Lateral view of half of concretion 1 (YPM 226437), showing location of center-edge transect sampled, the light area marked with x. The anomalocaridid specimen occurs in the top of this sample, perpendicular to the field of view. B, C) Top view of part (B) and counterpart (C) of anomalocaridid trunk segments preserved in concretion 2 (YPM 226438). Lines marked with x indicate the locations of perpendicular cuts where center-edge samples were removed. D) Detail of oxide pseudomorphs after pyrite in contact with the fossil specimen preserved in concretion 1.

Delta V mass spectrometer at the University of California, Riverside, with a standard deviation no larger than 0.2‰ for both carbon and oxygen.

It was necessary to combine some sample powders (B4 and 5; C4 and 5, discussed below) to provide enough material for XRF analysis. Thus, 21 samples were prepared as fused glass beads following the method of Johnson et al. (1999): 3.5 g of sample was mixed with 7.0 g of a lithium tetraborate flux, fused in graphite crucibles at 1000 °C for ten minutes and left to cool at room temperature to form glass beads. These beads were then re-powdered and fused a second time at 1000 °C. Following the second fusion, the glass beads were polished, cleaned by ultrasound, and analyzed for major and minor element chemistry using a Panalytical Axios XRF instrument at Pomona College.

X-radiographs of slabs taken from each of the three radial transects were prepared using a Faxitron cabinet X-radiograph system at Pomona College. Samples were irradiated at 60 kV for 50 minutes and the films were developed by hand.

Samples were analyzed by SEM-EDS using a Zeiss Leo 982 FE-SEM and a Bruker QUANTAX energy dispersive X-ray spectrometer at Pomona College. Freshly broken samples for textural analysis were coated with carbon prior to imaging at 5–15 kV. Chips used for elemental mapping were polished but not coated. Collection times for elemental maps ranged from 20 to 120 minutes.

RESULTS

Petrographic, mineralogic, and geochemical analysis of samples in the center-to-edge transects revealed that they are strikingly uniform in texture and composition across individual concretions, and between the two large concretions.

Composition

Mineralogic (XRD) data revealed the presence of only three mineral phases in each of the 23 samples analyzed: quartz, Fe-rich chlorite, and calcite, in order of decreasing abundance. Although XRD data are not quantitative, the relative intensities of the primary diffraction peaks of each mineral approximate the relative abundance of each mineral phase (Table 1). The primary variation in the data set is in the abundance of calcite, which is consistently more prominent in samples from concretion 1 than concretion 2. Petrographic and SEM data show that the abundance of calcite in concretion 2 has not been conspicuously reduced by weathering: no voids or dissolution pits are present within the samples. Although the ratio of the 001 peak of calcite to quartz is different between concretions 1 and 2, a radial (center-to-edge) trend in calcite:quartz is apparent in only one of the three transects (the part of concretion 2: YPM 226438). The ratio of the 002 diffraction peak of chlorite (the primary peak for Fe-rich chlorite) to the 001 peak of quartz is similar in all samples, and no radial trend is present.

Macroscopic (mm-scale) oxide pseudomorphs after pyrite are abundant at the center of concretions, in contact with the fossil specimens (Fig. 2D). However, the distribution of pyrite is strongly localized in the immediate vicinity of the fossils. Analysis of thin sections revealed that oxide pseudomorphs after pyrite are rare in the matrix of the concretions, and less than 20 μm in diameter. XRD detected neither pyrite nor Fe-oxide minerals in the matrix.

Whole-rock geochemistry (XRF) confirmed that the major element composition of the concretions is consistent across radial transects and is similar between concretions (Table 2). The primary difference in major element chemistry between concretions 1 and 2 results from the

TABLE 1—Raw peak intensity data for the primary peaks of quartz, chlorite, and calcite, as determined by XRD. Samples labeled A belong to a radial transect across concretion 1 (YPM 226437), B and C belong to transects across the part and counterpart, respectively, of concretion 2 (YPM 226438). Samples A1, B1 and C1 lie close to the center of the concretions, samples A12, B5, and C5 lie at concretion edges. Ratios of the raw intensities of the chlorite 002 peak and the calcite 001 peak to the 001 peak of quartz are also given, and show similar relative abundances of minerals across each of the three transects.

		Sample	Chlorite 002	Quartz 001	Calcite 001	Ch:Qtz	Ca:Qtz
Concretion 1	Center	A1	1750	4300	1900	0.41	0.44
		A2	800	1800	750	0.44	0.42
		A3	725	1800	750	0.40	0.42
		A4	700	1475	775	0.47	0.53
		A5	650	1375	775	0.47	0.56
		A6	525	1375	700	0.38	0.51
		A7	775	1800	800	0.43	0.44
		A8	700	1600	750	0.44	0.47
		A9	725	1850	600	0.39	0.32
		A10	725	1800	750	0.40	0.42
		A11	725	1775	775	0.41	0.44
	Edge	A12	700	1775	800	0.39	0.45
Concretion 2	Center	B1	800	2300	550	0.35	0.24
		B2	800	2375	525	0.34	0.22
		B3	725	2450	525	0.30	0.21
		B4	750	2400	450	0.31	0.19
	Edge	B5	900	2500	400	0.36	0.16
	Center	C1	700	2200	600	0.32	0.27
		C2	850	2550	650	0.33	0.25
		C3	625	1950	450	0.32	0.23
		C4	800	2400	550	0.33	0.23
	Edge	C5	875	2400	600	0.36	0.25

smaller weight percent calcite in concretion 2. Thus, the abundance of CaO is diminished in concretion 2 samples relative to those of concretion 1, while SiO_2, Fe_2O_3, and Al_2O_3 are proportionally enriched in concretion 2 samples. The ratios of both Fe_2O_3:SiO_2 and Al_2O_3:SiO_2 are greater in concretion 1 than in concretion 2, indicating a greater chlorite to quartz ratio in concretion 1 samples, as also indicated by XRD (Table 1) and SEM analyses. No radial trends in whole-rock chemistry were detected in any of the three transects sampled. The ratio of Al_2O_3:Fe_2O_3 is highly consistent among all samples, indicating that these phases reside primarily in chlorite. No significant pyrite is present in the matrix of the concretions; it is confined to the immediate vicinity of the fossil specimens. Major element data are consistent with XRD results: they show no evidence for the presence of mineral phases other than those detected by XRD.

Fabric

The fabric of the concretions was analyzed at the meso-micro scale (centimeters–microns) using X-radiography, acetate peels, thin sections, SEM imaging, and SEM-EDS elemental mapping. X-radiographs, thin sections and acetate peels revealed no evidence for radial growth fabrics, relict or replaced bedding, or center-to-edge compositional trends, as confirmed by the results of the compositional analyses described above.

SEM-EDS elemental mapping, in combination with analysis of thin sections, acetate peels, and SEM imaging, revealed that both concretions are characterized by randomly ordered microscopic (~10–100 μm) domains dominated by authigenic quartz (Si in the absence of Fe, Al, and Ca), Fe chlorite (Fe, Al, and Si), or calcite (Ca in the absence of Si, Fe, and Al) (Fig. 3). These domains are comprised of ultrafine-grained crystals (2–20 μm) (Fig. 4) and display intergrowth at their margins. The domains are not mineralogically homogenous, as elemental mapping revealed that all three minerals occur within domains dominated by one of the others (Fig. 3). Analysis of samples taken radially indicated that neither the distribution and size of these domains, nor the size ranges and distribution of individual authigenic mineral crystals, vary across radial transects.

Isotope Geochemistry of Calcite

$\delta^{13}C$ values (Table 3) are prominently negative in all samples (range: −9.4‰ to −15.1‰; avg. −12.2‰), indicating a substantial contribution of organically derived bicarbonate to the pore waters from which the calcite precipitated (e.g., Coleman, 1985). $\delta^{18}O$ values exhibit a narrow range (−10.5‰ to −13.0‰; avg. −11.8‰) typical of early Paleozoic carbonates (Jaffres et al., 2007).

Radial trends in $\delta^{13}C$ values are prominent in each of the three transects analyzed from the two concretions, displaying a variation of

TABLE 2—Bulk elemental composition of samples from the three radial transects, as determined by XRF. Ratios of major primary elemental abundances (Al, Fe, Si, Ca) show consistently similar values across individual transects.

		Sample	SiO_2 (%)	TiO_2 (%)	Al_2O_3 (%)	Fe_2O_3 (%)	MgO (%)	MnO (%)	CaO (%)	K_2O (%)	Na_2O (%)	P_2O_5 (%)	Al:Si	Fe:Si	Fe:Al	Ca:Si
Concretion 1	Center	A1	45.18	0.39	9.11	14.95	2.27	0.49	12.83	0.15	0.08	0.08	0.202	0.331	0.609	0.284
		A2	45.46	0.41	9.46	15.64	2.39	0.37	12.9	0.2	0.19	0.08	0.208	0.344	0.605	0.284
		A3	44.49	0.4	9.16	15.31	2.32	0.4	13.33	0.14	0.15	0.08	0.206	0.344	0.598	0.300
		A4	43.89	0.4	9.06	15.47	2.34	0.41	14.16	0.12	0.14	0.09	0.206	0.352	0.586	0.323
		A5	44.05	0.4	9.05	15.33	2.37	0.38	13.97	0.11	0.11	0.09	0.205	0.348	0.590	0.317
		A6	43.98	0.41	9.26	15.36	2.38	0.41	13.43	0.12	0.09	0.09	0.211	0.349	0.603	0.305
		A7	45.87	0.41	9.4	15.74	2.45	0.4	12.81	0.14	0.13	0.1	0.205	0.343	0.597	0.279
		A8	46.08	0.4	9.25	15.32	2.42	0.38	12.94	0.13	0.13	0.1	0.201	0.332	0.604	0.281
		A9	45.73	0.41	9.22	14.91	2.4	0.37	12.86	0.1	0.03	0.12	0.202	0.326	0.618	0.281
		A10	46.6	0.39	8.94	15.56	2.37	0.36	12.69	0.08	0.19	0.09	0.192	0.334	0.575	0.272
		A11	44.92	0.41	8.98	16.05	2.37	0.5	13.2	0.08	0.23	0.06	0.200	0.357	0.560	0.294
	Edge	A12	44.73	0.38	8.69	15.12	2.3	0.41	13.45	0.04	-0.03	0.05	0.194	0.338	0.575	0.301
		AU	47.98	0.45	10.15	14.03	2.3	0.33	10.43	0.67	0.1	0.46	0.212	0.292	0.723	0.217
Concretion 2	Center	B1	57.66	0.42	9.7	16.09	2.51	0.27	4.8	0.09	0.01	0.27	0.168	0.279	0.603	0.083
		B2	58.81	0.43	9.9	17	2.59	0.16	4.48	0.1	0.15	0.24	0.168	0.289	0.582	0.076
		B3	58.32	0.42	10.09	16.1	2.59	0.17	4.36	0.14	-0.02	0.2	0.173	0.276	0.627	0.075
	Edge	B4-5	60.6	0.45	10.51	16.34	2.58	0.16	3.14	0.34	0.12	0.12	0.173	0.270	0.643	0.052
	Center	C1	56.3	0.38	8.74	15.12	2.27	0.31	6.78	0.03	-0.01	0.14	0.155	0.269	0.578	0.120
		C2	57.99	0.38	9.03	16.17	2.39	0.26	6.15	0.06	0.2	0.29	0.156	0.279	0.558	0.106
		C3	56.63	0.4	9.32	15.38	2.44	0.21	6.25	0.06	0.03	0.4	0.165	0.272	0.606	0.110
	Edge	C4-5	57.96	0.41	9.48	16.18	2.48	0.24	5.66	0.1	0.1	0.17	0.164	0.279	0.586	0.098

up to 4.6‰ from center to edge. The two transects measured across concretion 2 are essentially symmetrical, with identical $\delta^{13}C$ values from near center (−9.4‰) and opposite edge samples (−11.3‰). While $\delta^{13}C$ transects across concretion 2 become more negative toward the edge, $\delta^{13}C$ values across the transect from concretion 1 become more positive toward the edge (−15.1‰ to −10.5‰).

DISCUSSION

The Fezouata anomalocaridids were preserved by the growth of a mineral matrix around a decomposing carcass, which preserved the gross morphology. The fine intergrowth and morphology of the three mineral phases, quartz, Fe chlorite, and calcite, clearly indicate an authigenic origin; there is no evidence of detrital sediment within concretion matrices. Chlorite occurs in well-ordered books with Z-axes that approach and often exceed both the X- and Y-axes in length (Figs. 4C–E); in contrast, detrital clays are characterized by a sheet-like morphology with Z-axes much shorter than X- and Y-axes (O'Brien and Slatt, 1990). Quartz grains display irregular facets produced by poorly ordered silica growing against crystallites of calcite or authigenic clay (Figs. 4E–F), precluding the possibility of a detrital origin. The strongly negative $\delta^{13}C$ values of calcite and its rhombohedral morphology also indicate diagenetic precipitation.

The absence of relict sedimentary fabrics (confirmed by X-radiography, thin section, acetate peel, and SEM-EDS analysis) and of detrital sediment grains indicates that the Fezouata concretions grew pervasively at, or near, the sediment-water interface without incorporating any detectable detrital fraction. The replication of aspects of soft-bodied anatomy in three dimensions requires precipitation of mineral products in areas immediately surrounding those labile tissues on a timescale of weeks to months (Briggs and Kear, 1994). Furthermore, the compositional (Tables 1–2) and textural (Fig. 3) homogeneity of the concretions, as well as their ultrafine grain size and the absence of concentric growth fabrics, is noteworthy. This suggests that the geochemical conditions that favored mineral precipitation in the early entombment environment, including pH and ionic strength of pore fluids, were maintained during growth of the entire concretions. Thus, we infer that the framework of the concretions grew rapidly around the decomposing carcasses. In order to retain anatomical detail, specifically the three-dimensionality of gill branches, the mineral matrix must have precipitated around a carcass prior to the collapse of the soft tissues resulting from decay (Briggs and Kear, 1994). Growth of the concretions, however, may have continued long after replication of the details of nonbiomineralized tissue anatomy was complete.

The precipitation of authigenic pyrite around labile tissues requires an anaerobic environment in which microbial activity is elevated around carcasses in sediments that are otherwise organic poor (Briggs et al., 1991, 1996; Canfield and Raiswell, 1991; Raiswell et al., 2008), a condition that establishes prominent chemical gradients around a potential fossil. The formation of the concretion required abundant sources of SiO_2, Al^{3+}, Fe^{2+}, Mg^{2+}, Ca^{2+}, and HCO_3^- in the adjacent pore waters. HCO_3^- was supplied by vigorous bacterial sulfate reduction of labile organic tissues, as also indicated by the $\delta^{13}C$ values of calcite (Table 3); sufficient Ca^{2+} to precipitate calcite could have been supplied from seawater, although contributions from other sources are not excluded. However, the cations required for precipitation of large volumes of silica and Fe chlorite were unlikely to have been present in large concentrations in seawater, and must have been derived from the sediments.

Early diagenetic (low-temperature) silica can originate from dissolution of three sources within marine mudstone: (1) biogenic opaline silica; (2) clay minerals via the activity of iron-reducing bacteria; or (3) volcanic ash (Schieber et al., 2000; Vorhies and Gaines, 2009). Dissolution of biogenic silica from sponge spicules and possibly radiolarian tests may have contributed to the silica in the concretions but it is unlikely that the local volume of these components would have been sufficient. Nor can the dissolution of biogenic silica account for the high concentrations of Al^{3+}, Fe^{2+}, and Mg^{2+} required for Fe-chlorite precipitation. Microbially mediated dissolution of clay minerals may liberate these cations and has been proposed as a source of silica for cm-scale chert nodules of the Doushantuo Formation (Xiao et al., 2010). It is unlikely, however, that the volume of clay dissolved through microbial activity (Vorhies and Gaines, 2009) would have been sufficient to precipitate the Fezouata concretions over the short timescale required. The exclusion of these two sources of early diagenetic silica suggests that the concretions may have precipitated from ions derived from the dissolution of volcanic ash, although diagenetic alteration and weathering of the host sediments make

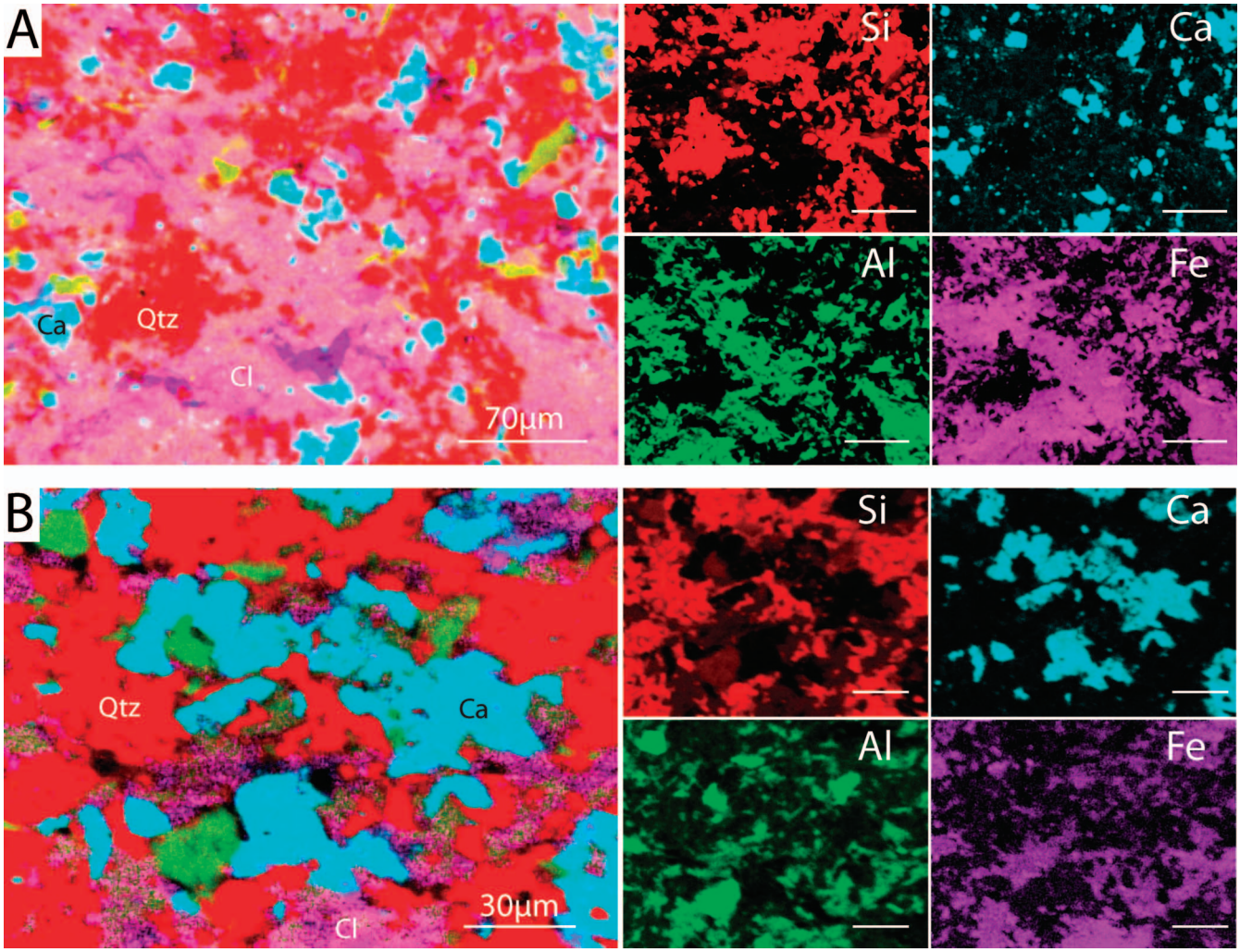

FIGURE 3—SEM-EDS elemental maps showing the mineral fabric of the concretion matrix and mineral phase relationships (concretion 2: YPM 226438). In both sets of images, a composite elemental map of Si, Ca, Al, and Fe is shown at left with smaller individual maps for each element shown at right. Examples of domains dominated by Qtz = quartz, Cl = chlorite, and C = calcite are marked on the composite maps. A) Field of view showing multiple 10–100 µm domains dominated by each of the three mineral phases. Quartz domains appear bright red, chlorite domains appear pink, and calcite domains appear blue. Note that domains dominated by each of the three minerals contain inclusions of the other two mineral phases. While elemental maps for Al and Fe are overlapping to a large extent, regions dominated by each appear on the composite map, revealing regions of chlorite with elevated Al (green) or Fe (purple) content relative to the dominant composition of the matrix chlorite, as also seen in B, below. B) Higher magnification field of view illustrating fine-scale textural relationships among mineral domains. Note intergrowth of mineral phases within and at the margins of domains.

definitive identification of a precursor ash phase difficult. Ash is comprised largely of Al-bearing metastable glass shards and is susceptible to dissolution with a decline in pH (Duggen et al., 2010; Ayris and Delmelle, 2011) such as accompanies the decay of carcasses (Coleman, 1985; Sagemann et al., 1999). Volcanic deposits intercalated with mudstone of the lower Fezouata Formation were generated during tectonic activity associated with the rifting of Avalonia from the Gondwanan margin (Tahiri et al., 2010) in the study area (eastern Anti-Atlas: Destombes et al., 1985; Pique and Michard, 1989). While the original presence of ash in the horizons bearing the concretions cannot be established with certainty, alternative low-temperature sources of silica are insufficient to account for the large volume of the concretions, nor could they have supplied the other cations required for the precipitation of Fe chlorite. Given the absence of a viable alternative scenario, we consider it likely that volcanic ash comprised a significant component of the substrate, supplied to the basin either as concentrated detrital volcaniclastic material or as airfall from local eruptions.

Shortly after the giant carcasses were buried, vigorous sulfate reduction began, as evidenced by abundant pyrite now altered to oxide pseudomorphs (Fig. 2D). Sulfate reduction coincident with pyrite precipitation would have led to a localized drop in pH (Birnbaum and Wireman, 1984; Coleman, 1985; Sagemann et al., 1999; Xiao et al., 2010) and would have promoted dissolution of the implied volcanic ash precursor phase (Duggen et al., 2010; Ayris and Delmelle, 2011). The introduction of volcanic ash to seawater results in a localized decline in pH and the liberation of major cations from ash to solution (Duggen et al., 2010). Whether promoted by recent introduction of ash to the seafloor environment, or by a pH drop associated with microbial degradation of labile tissues, the dissolution of an ash phase would have resulted in the release of SiO_2, Al^{3+}, Fe^{2+}, Mg^{2+}, and potentially other ions including Ca^{2+} and K^+, to pore waters. The pore waters were iron dominated, as evidenced by the localization of pyrite (Briggs et al., 1991, 1996; Canfield and Raiswell, 1991; Raiswell et al., 2008) and the precipitation of abundant Fe chlorite. As sulfate reduction proceeded, the production of bicarbonate led to a recovery of pH and promoted rapid precipitation of intergrown minerals that formed the framework of the concretions and grew around the fossils, preserving the outlines of nonbiomineralized tissues as mineral overgrowth. It is likely that silica precipitated initially as amorphous or poorly ordered SiO_2, which was later converted to quartz during burial. Although Fe chlorite may precipitate directly from pore waters during

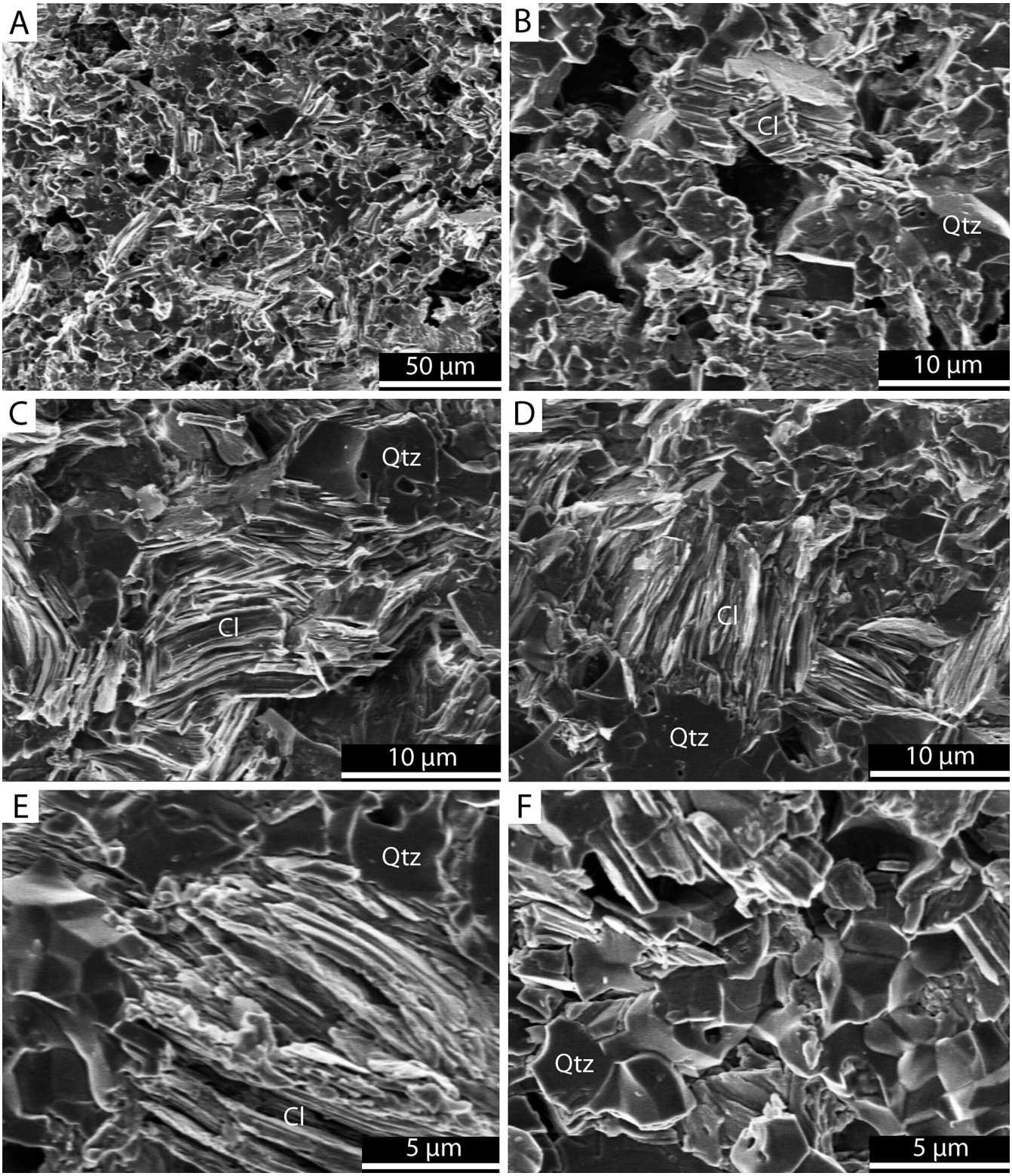

FIGURE 4—Scanning electron micrographs of freshly broken samples of concretion 2 (YPM 226438), illustrating texture of the concretion matrices, and morphology and textural relationships of quartz (=Qtz) and chlorite (=Cl) crystals. Samples were etched with HCl to remove calcite, resulting in void spaces that appear dark. Chlorite is recognized by its prominent layered structure. Quartz grains are blocky and often display fracture. A, B) Concretion matrix fabric, showing very fine crystallite size of the matrix (2–20 µm), and voids revealing the primary distribution of calcite throughout the matrix of concretion 2. C, D) Intergrown authigenic quartz and chlorite in concretion 2. E, F) Irregular polygonal faces evident on quartz crystals in concretion 1 indicating growth against other mineral grains.

early diagenesis (Burton et al., 1987) it forms more commonly from burial recrystallization of precursor Fe-clay phases, such as odinite (Grigsby, 2001). Thus, we infer that localized pH changes accompanying anaerobic decay of the unusually large invertebrate carcasses led first to dissolution of ash in the substrate and secondly to the precipitation of the silicate mineral frameworks.

Calcite, a minor component of the Fezouata concretions, may have precipitated at the same time as the other two phases. Simultaneous

TABLE 3—$\delta^{13}C$ and $\delta^{18}O$ values of calcite from each of the three radial transects.

		Sample	$\delta^{13}C$ (‰-VPDB)	$\delta^{18}O$ (‰-VPDB)
Concretion 1	Center	A1	-15.1	-11.5
		A2	-14.3	-10.7
		A3	-14.6	-10.5
		A4	-14.8	-11.6
		A5	-15.0	-12.1
		A6	-14.6	-12.7
		A7	-13.2	-12.4
		A8	-13.6	-12.6
		A9	-14.2	-13.0
		A10	-12.2	-12.7
		A11	-11.4	-11.4
	Edge	A12	-10.5	-11.5
		A unknown	-13.5	-11.2
Concretion 2	Center	B1	-9.4	-11.4
		B2	-9.6	-11.6
		B3	-10.5	-12.3
		B4	-10.5	-11.6
	Edge	B5	-11.3	-12.4
	Center	C1	-9.4	-10.9
		C2	-9.6	-11.5
		C3	-11.4	-12.1
		C4	-10.6	-12.1
	Edge	C5	-11.3	-11.5

growth is suggested by the fine intergrowth of calcite with quartz and Fe chlorite (Fig. 3). However, it is also possible that calcite precipitated as a pore-filling phase after precipitation of the quartz-chlorite framework, following an increase in pH. Strongly depleted $\delta^{13}C$ values clearly indicate that calcite precipitated from a pool of bicarbonate largely generated from decomposition of the large carcasses and other organic material in the sediments. Radial trends in the $\delta^{13}C$ values of calcite may reflect mixing of seawater-derived bicarbonate with that derived from anaerobic decomposition of the carcasses during rapid, pervasive cementation, or these trends may have resulted from radial growth of a pore-filling calcite cement within the quartz-chlorite framework. Variation in $\delta^{18}O$ across radial transects is small and nondirectional suggesting rapid pervasive cementation rather than radial precipitation across a geothermal temperature gradient. However, given the opposite center-edge trends in $\delta^{13}C$ between the two concretions, investigation of additional concretions is required to refine our understanding of the process.

CONCLUSION

The quartz-chlorite-calcite composition of the Fezouata concretions is unlike that of other examples described from marine environments, and may be unique. Their growth, which resulted in the exceptional preservation of the giant anomalocaridids, required special circumstances of authigenesis, promoted by a highly reactive sediment composition and the delivery of large carcasses to the seafloor in otherwise organic-poor sediments. The mineralogic composition of the concretions suggests a substrate that was rich in volcanic ash, an interpretation supported by the presence of volcanic deposits within the lower Fezouata Formation (Destombes, et al., 1985; Pique and Michard, 1989). Vigorous microbial sulfate reduction of labile tissues of the large carcasses established steep chemical gradients that led to rapid dissolution of ash in the sediments. This resulted in liberation of cations that precipitated rapidly as silica and Fe-rich clay around the non bio-mineralized tissues. Limited intergrown calcite precipitated from a pool of $\delta^{13}C$-depleted bicarbonate supplied primarily by sulfate reduction of the carcasses themselves. Exceptional preservation within the concretions resulted from advanced microbial decomposition of organic tissues that, in this case, led to rapid mineralization and replication of nonbiomineralized anatomy.

ACKNOWLEDGMENTS

We thank M. Ben Moula, J. Botting, L. Muir, J. Vinther, and C. Upton for assistance in the field. L. Ben Moula and B. Tahiri provided logistic support. S. Butts and U. Farrell provided valuable assistance with study material from Yale Peabody Museum collections, and L. Curtin and N. Schweitzer assisted with sample preparation and XRF analysis. Fieldwork benefited from a National Geographic Society Research and Exploration Grant. This work was supported by National Science Foundation (NSF) EAR-1053247 to DEGB. Analytical work was also supported by NSF DMR-0618417 and NSF DUE-0942447 to RRG. Parts of the work were undertaken while PVR was in receipt of Irish Research Council for Science, Engineering, and Technology (IRCSET) and Ghent University BOF (Special Research Fund) Postdoctoral Fellowship grants.

REFERENCES

Allison, P.A., and Pye, K., 1994, Early diagenetic mineralization and fossil preservation in modern carbonate concretions: PALAIOS, v. 9, p. 561–575.

Ayris, P., and Delmelle, P., 2011, Volcanic and atmospheric controls on ash iron solubility: A review: Physics and Chemistry of the Earth, doi: 10.1016/j.pce.2011.04.013.

Berner, R.A., 1968, Calcium carbonate concretions formed by the decomposition of organic matter: Science, v. 159, p. 195–197.

Birnbaum, S.J., and Wireman, J.W., 1984, Bacterial sulfate reduction and pH: Implications for early diagenesis: Chemical Geology, v. 43, p. 143–149.

Briggs, D.E.G., 2003, The role of decay and mineralization in the preservation of soft-bodied fossils: Annual Reviews in Earth and Planetary Science, v. 31, p. 275–301.

Briggs, D.E.G., and Kear, A.J., 1994, Decay and mineralization of shrimps: PALAIOS, v. 9, p. 431–456.

Briggs, D.E.G., Bottrell, S.H., and Raiswell, R., 1991, Pyritization of soft-bodied fossils: Beecher's Trilobite Bed, Upper Ordovician, New York State: Geology, v. 19, p. 1221–1224.

Briggs, D.E.G., Raiswell, R., Bottrell, S. H., Hatfield, D., and Bartels, C., 1996, Controls on the pyritization of exceptionally preserved fossils: An analysis of the Lower Devonian Hunsrück Slate of Germany: American Journal of Science, v. 296, p. 633–663.

Burton, J.H., Krinsley, D.H., and Pye, K., 1987, Authigenesis of kaolinite and chlorite in Texas Gulf Coast sediments: Clays and Clay Minerals, v. 35, p. 291–296.

Butterfield, N.J., 1995, Secular distribution of Burgess Shale-type preservation: Lethaia, v. 28, p. 1–13.

Butterfield, N.J., 2003, Exceptional fossil preservation and the Cambrian explosion: Integrative and Comparative Biology, v. 43, p. 166–177.

Canfield, D.E., and Raiswell, R., 1991, Pyrite formation and fossil preservation, *in* Allison, P.A., and Briggs, D.E.G., eds., Taphonomy: Releasing the Data Locked in the Fossil Record: Plenum Press, New York, p. 337–387.

Ciampaglio, C.N., Babcock, L.E., Wellman, C.L., York, A.R., and Brunswick, H.K., 2006, Phylogenetic affinities and taphonomy of *Brooksella* from the Cambrian of Georgia and Alabama, USA: Palaeoworld, v. 15, p. 256–265.

Cocks, L.R.M., and Torsvik, T.H., 2006, Major terranes in the Ordovician, *in* Webby, B.D., Paris, F., Droser, M.L., and Percival, I.G., eds., The Great Ordovician Biodiversification Event: Columbia University Press, New York, p. 61–67.

Coleman, M.L., 1985, Geochemistry of diagenetic non-silicate minerals: Kinetic considerations: Philosophical Transactions of the Royal Society of London A, v. 315, p. 39–56.

Destombes, J., Hollard, H., and Willefer, S., 1985, Lower Paleozoic rocks of Morocco, *in* Holland, C.H., ed., Lower Paleozoic of North-Western and West-Central Africa: John Wiley and Sons, New York, p. 91–336.

Duggen, S., Olgun, N., Hoffman, L., Dietze, H., Delmelle, P., and Teschner, C., 2010, The role of airborne volcanic ash for the surface ocean biogeochemical iron-cycle: A review: Biogeosciences, v. 7, p. 827–844.

Finnegan, S., Bergmann, K., Eiler, J.M., Jones, D.S., Fike, D.A., Eisenman, I., Hughes, N.C., Tripati, A.K., and Fischer, W.W., 2011, The magnitude and duration of Late Ordovician-Early Silurian glaciation: Science, v. 331, p. 903–906.

Gaines, R.R., Kennedy, M.J., and Droser, M.L., 2005, A new hypothesis for organic preservation of Burgess Shale taxa in the Middle Cambrian Wheeler Shale, House Range, Utah: Palaeogeography, Palaeoclimatology, Palaeoecology, v. 220, p. 193–205.

Gaines, R.R., Briggs, D.E.G., and Zhao, Y.L., 2008, Burgess Shale-type deposits share a common mode of fossilization: Geology, v. 36, p. 755–758.

Grigsby, J.D., 2001, Origin and growth mechanism of authigenic chlorite in sandstones of the lower Vicksburg Formation, south Texas: Journal of Sedimentary Research, v. 71, p. 27–36.

Huggett, J.M., Gale, A.S., and Evans, S., 2000, Carbonate concretions from the London Clay (Ypresian, Eocene) of southern England and the exceptional preservation of wood-boring communities: Journal of the Geological Society, v. 157, p. 187–200.

Jaffres, J.B.D., Shields, G.A., and Wallman, K., 2007, The oxygen isotope evolution of seawater: A critical review of a long-standing controversy and an improved geological water cycle model for the past 3.4 billion years: Earth Science Reviews, v. 83, p. 83–122.

Johnson, D.M., Hooper, P.R., and Conrey, R.M., 1999, XRF analysis of rocks and minerals for major and trace elements on a single low dilution Li-tetraborate fused bead: Advances in X-Ray Analysis: v. 41, p. 843–867.

Maas, A., Braun, A., Dong, X.-P., Donoghue, P.C.J., Müller, K.J., Olempska, E., Repetski, J.E., Siveter, D.J., Stein, M., and Waloszek, D., 2006, The "Orsten": More than a Cambrian Konservat-Lagerstätte yielding exceptional preservation: Palaeoworld, v. 15, p. 266–282.

Maeda, H., Tanaka, G., Shimobayashi, N., Ohno, T., and Matsuoka, H., 2011, Cambrian Orsten Lagerstätte from the Alum Shale Formation: Fecal pellets as a probable source of phosphorus preservation: PALAIOS, v. 26, p. 225–231.

Mapes, R.H., 1987, Upper Paleozoic cephalopod mandibles: Frequency of occurrence, modes of preservation, and paleoecological implications: Journal of Paleontology, v. 61, p. 521–538.

Martill, D.M., 1988, Preservation of fish in the Cretaceous Santana Formation of Brazil: Palaeontology, v. 31, p. 1–18.

O'Brien, N.R., and Slatt, R.M., 1990, Argillaceous Rock Atlas, Springer-Verlag: New York, 141 p.

Orr, P.J., Briggs, D.E.G., Siveter, D.J., and Siveter, D.J., 2000, Three-dimensional preservation of a non-biomineralized arthropod in concretions in Silurian volcaniclastic rocks from Herefordshire, England: Journal of the Geological Society, v. 157, p. 173–186.

Park, L.E., 1995, Geochemical and paleoenvironmental analysis of lacustrine arthropod-bearing concretions of the Barstow Formation, southern California: PALAIOS, v. 10, p. 44–57.

Petrovich, R., 2001, Mechanisms of fossilization of the soft-bodied and lightly armored faunas of the Burgess Shale and of some other classical localities: American Journal of Science, v. 301, p. 683–726.

Pique, A., and Michard, A., 1989, Moroccan Hercynides: A synopsis. The Paleozoic sedimentary and tectonic evolution at the northern margin of west Africa: American Journal of Science, v. 289, p. 286–330.

Pye, K., Dickson, J.A.D., Schiavon, N., Coleman, M., and Cox, M., 1990, Formation of siderite-Mg-calcite-iron sulphide concretions in intertidal marsh and sandflat sediments, north Norfolk, England: Sedimentology, v. 37, p. 325–343.

Raiswell, R., 1987, Non-steady state microbiological diagenesis and the origin of concretions and nodular limestones: Geological Society of London Special Publication, v. 36, p. 41–54.

Raiswell, R., and Fisher, O.J., 2000, Mudrock-hosted carbonate concretions: A review of growth mechanisms and their influence on chemical and isotopic composition: Journal of the Geological Society, v. 157, p. 239–251.

Raiswell, R., Newton, R., Bottrell, S.H., Coburn, P.M., Briggs, D.E.G., Bond, D.P., and Poulton, S.W., 2008, Turbidite depositional influences on the diagenesis of Beecher's Trilobite Bed and the Hunsrück Slate; sites of soft tissue pyritization: American Journal of Science, v. 308, p. 105–129.

Rice, C.M., Trewin, N.H., and Anderson, L.I., 2002, Geological setting of the Early Devonian Rhynie Cherts, Aberdeenshire, Scotland: An early terrestrial hot spring system: Journal of the Geological Society, v. 159, p. 203–214.

Sagemann, J., Bale, S.J., Briggs, D.E.G., and Parkes, R.J., 1999, Controls on the formation of authigenic minerals in association with decaying organic matter: An experimental approach: Geochimica Cosmochimica Acta, v. 63, p. 1083–1095.

Schieber, J., Krinsley, D., and Riciputi, L., 2000, Diagenetic origin of quartz silt in mudstones and implications for silica cycling: Nature, v. 406, p. 981–985.

Schopf, J.W., 1993, Microfossils of the Early Archean Apex Chert: New evidence of the antiquity of life: Science, v. 260, p. 640–646.

Schwimmer, D.R., and Montante, W.M., 2007, Exceptional fossil preservation in the Conasauga Formation, Cambrian, northwestern Georgia, USA: PALAIOS, v. 22, p. 360–372.

Sellés-Martínez, J., 1996, Concretion morphology, classification and genesis: Earth Science Reviews, v. 41, p. 177–210.

Tahiri, A., Montero, P., El Hadi, H., Poyatos, D.M., Azor, A., Bea, F., Simancass, J.F., and Lodeiro, F.G., 2010, Geochronological data on the Rabat-Tiflet granitoids: Their bearing on the tectonics of the Moroccan Variscides: Journal of African Earth Sciences, v. 57, p. 1–13.

Van Roy, P., and Briggs, D.E.G., 2011, A giant Ordovician anomalocaridid: Nature, v. 473, p. 510–513.

Van Roy, P., Orr, P.J., Botting, J.P., Muir, L.A., Lefebvre, B., El Hariri, K., and Briggs, D.E.G., 2010, Ordovician faunas of Burgess Shale type: Nature, v. 465, p. 215–218.

Vorhies, J.S., and Gaines, R.R., 2009, Microbial dissolution of clay minerals as a source of iron and silica in marine sediments: Nature Geoscience, v. 2, p. 221–225.

Wilby, P.R., and Martill, D.M., 1992, Fossil fish stomachs: A microenvironment for exceptional preservation: Historical Biology, v. 6, p. 25–36.

Xiao, S., Schiffbauer, J.D., Mcfadden, K.A., and Hunter, J., 2010, Petrographic and SIMS pyrite sulfur isotope analyses of Ediacaran chert nodules: Implications for microbial processes in pyrite rim formation, silicification, and exceptional fossil preservation: Earth and Planetary Science Letters, v. 297, p. 481–495.

Zhang, X.-G., Siveter, D.J., Waloszek, D., and Maas, A., 2007, An epipodite-bearing crown-group crustacean from the Lower Cambrian: Nature, v. 449, p. 595–598.

ACCEPTED JANUARY 17, 2012